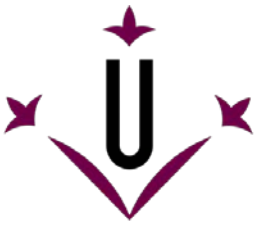

Numerical analysis of a latent heat thermal energy storage system under partial load operating conditions

Simone Arena[1,*], Efisio Casti[1], Jaume Gasia[2], Luisa F. Cabeza[2], Giorgio Cau[1]
[1]Dept. of Mechanical, Chemical and Materials Engineering, University of Cagliari, Via Marengo 2, 09123, Cagliari, Italy
[2]GREiA Research Group, INSPIRES Research Centre, University of Lleida, Pere de Cabrera s/n, 25001, Lleida, Spain

Abstract

One of the features that should be considered when designing a thermal energy storage (TES) system is its behaviour when subjected to non-continuous (partial loads) operating conditions. Indeed, the system performance can be sensibly affected by the partial charging and discharging processes. This topic is analysed in the present study by means of a two-dimensional axisymmetric numerical model implemented in COMSOL Multiphysics. A latent heat TES system consisting of a vertical concentric tube heat exchanger is simulated to investigate the effect of different partial load operating conditions on the system behaviour.
The effects of different heat transfer distributions and evolutions of the solid-liquid interface, are evaluated to identify the optimal management criteria of the TES systems. The results showed that partial load strategies allow to achieve a substantial reduction in the duration of the TES (up to 50%) process against a small decrease in stored energy (up 30%). The close correlation between the energy and the duration of the TES cycle is also evaluated during the discharge using detailed maps related to the melting fraction. These maps allow for the evaluation of the most efficient load conditions considering both charging and discharging processes to satisfy a specific energy demand.

Keywords: Phase change material (PCM), Thermal energy storage (TES), Partial loads, Latent heat, Numerical simulation

* Corresponding author.
E-mail address: simonearena@unica.it

Nomenclature

Dimensional variables

A_{mush}	Mushy zone constant [kg/s]
A_{surf}	Heat transfer surface [m^2]
C_p	Specific heat capacity [J/kg·K]
d	Diameter [mm]
E	Energy [kWh]
F	Force [N]
g	Gravity acceleration [m/s^2]
H	Height [mm]
k	Thermal conductivity [W/m·K]
L_f	Latent heat of fusion [J/kg]
n	Unit vector normal of the section
P	Pressure [Pa]
s	Tube thickness [mm]
t	Time [s]
T	Temperature [K]
T_m	PCM phase change temperature [K]
u	Velocity [m/s]

Subscripts

ch	Charge phase
$disc$	Discharge phase
e	External
i	Internal
in	Inlet section
out	Outlet section
res	Residual

Greek symbols

α	Mass fraction
β	Thermal expansion coefficient [1/K]
ΔT_m	Phase change temperature range [K]
ϵ	Numerical constant
θ	Fraction of phase before transition
μ	Dynamic viscosity [Pa·s]
ρ	Density [kg/m^3]

Abbreviations

CSP	Concentrated solar power
HTF	Heat transfer fluid
$LHTES$	Latent heat thermal energy storage
MF	Melting fraction
ORC	Organic Rankine cycle
$PAFC$	Phosphoric acid fuel cells
PCM	Phase change material
ROE	Ratio of energy
TES	Thermal energy storage

1 Introduction

Thermal energy storage (TES) is a widely studied topic that represents an essential option in all systems characterised by their intermittent nature, such as solar energy, or those which require storage for later use. Thus, TES plays an important role in energy conservation and efficiency, improving the performance and reliability of energy systems, and decreasing peak-loads in the electrical grid. Among the different technological solutions, latent heat thermal energy storage (LHTES) systems with phase change materials (PCMs) represent a very interesting option, for a wide range of temperatures, in many applications for heating and cooling, and power generation processes. The main advantages of LHTES systems are high TES capacity per unit mass, compared to sensible heat TES systems, and a small operating temperature range [1].

In TES systems, energy is stored to be used afterwards, involving three steps: charge, storage and discharge, consisting of the complete storage cycle. However, during operation, it is not always necessary or possible to perform a complete storage cycle due to both the discontinuous availability of the energy source and, for example, to unexpected peak-loads, failures or random energy demand during time or simply is not suitable. Thus, in these cases, it is essential to provide the energy required even if, considering a LHTES system, the PCM inside the storage system has not yet reached the complete melting conditions or to recharge it starting from incomplete solidification conditions.

Generally, most of the studies of these systems have been based on complete charge and discharge cycles, in which the initial conditions of the two processes coincide with "stationary" conditions. The PCM is in a solid state at the beginning of the charging process (melting) and completely in a liquid state at the end of the charge, which is also the PCM state at the beginning of the discharging process (solidification). Nevertheless, the issue related to partial load storage strategies has mainly been treated by focusing on the optimisation of integrated TES systems to achieve the highest reduction in peak energy demand, while ensuring technical and economic feasibility. Hasnain et al. [2] studied a cool thermal energy storage coupled to a partial ice storage system in office buildings, attaining a reduction in the peak electrical power demand of up to 20% and in peak cooling load of up to 40%. Al-Qalamchi and Adil [3] investigated chiller size determination by adopting a combined strategy system that includes partial and full load conditions working simultaneously. They found that the combined strategy system leads to a reduction in chiller size of ~28%

compared to conventional systems, although only a partial strategy requires less chiller size than the combined system. Sanaye and Hekmatian [4] presented an air-conditioning system integrated in an ice TES system analysing energy, exergy, economic and environmental aspects under full and partial load conditions. The results showed that partial load operating conditions allow lower investment costs, payback time and savings in operating costs during system life time, when compared to full load operating conditions. Xu et al. [5] numerically investigated the behaviour of a variable mass energy transformation and storage system, using NH_3–H_2O as the working fluid, under full and partial storage strategies. They found that the full storage strategy is more suitable for small and domestic energy storage systems for cooling, heating and day-to-day hot water supply applications, while the partial storage strategy is more suitable for large- or mid-scale energy storage systems. Rahman et al. [6] presented a technical-economic analysis of cool TES systems for both full and partial storage scenarios in real building applications. The results showed that the full and partial chilled storage systems allow reductions of up to 61.19% and 50.26%, respectively, of the electricity cost required for cooling, when compared with conventional systems. Nithyanandam et al. [7] and Zhao et al. [8] presented an investigation of packed-bed TES systems for Concentrated Solar Power (CSP) plants performing full and partial load operating conditions. It was shown that the increase in partial load operating cycles leads to a decrease in energy storage and release capacity. Macphee and Dincer [9] presented a comparison of four types of ice storage techniques for space cooling purposes considering full and partial storage strategies. They found that the efficiency of these systems was slightly lower in partial loads than in the full load scenario due to higher heat leakage in the partial load operating conditions. Delcroix et al. [10] presented a comparison between experimental and numerical results of a wall section equipped with PCMs under partial load scenarios during both melting and solidification processes. The results showed that the PCM undergoes a rapid transition between the heating and cooling curves if the heating or cooling process is interrupted during phase change.

The foregoing discussion suggests that although several studies have been reported on different storage strategies, the literature on the performance of a LHTES system under partial load operating conditions for medium-to-high temperature applications is relatively limited. To this end, this study aims to deepen our understanding of the effect of partial load operating conditions in a TES system using a PCM for the temperature range between 150 and 220 °C, with particular reference to the influence on significant parameters, such as the energy stored and the time required to complete the storage process. In this temperature range, LHTES systems are typically applied in concentrating solar technologies associated with small size Organic Rankine Cycles (ORCs) [11–13] or industrial waste heat recovery systems [14]. Other applications are in solar cooling systems with absorption chillers [15], PAFC fuel cells [16], heat recovery in metal hydride hydrogen storage systems [17] in the food, beverage, transport equipment, textile, machinery, pulp and paper industries and drying of agricultural products [18]. To accomplish the purpose of the present study, a vertical concentric tube heat exchanger was selected as LHTES system based on the configuration of a prototype used for experimental tests at the University of Lleida (Spain) [19]. In the proposed paper, a numerical analysis of partial load effects using a mathematical model developed and validated in previous works considering the same experimental facility [20,21] was carried out. This analysis was specifically focused on the assessment of the entire cyclic storage process to optimise management of LHTES systems in real operating conditions in order to analyze the behaviour of these systems under partial load operating conditions. The results presented in this paper can help to provide an accurate decision-making strategy when LHTES systems are subjected to variable or discontinuous energy requirements. Thus, four different percentages values of state-of-charge of the TES system, which refers to the melting fraction value at the end of the charge and equal to 100% (baseline case), 95%, 90% and 75%, were selected. The effects of the partial load operating conditions were studied by analysing fundamental parameters, such as the energy stored/released during charging and discharging processes and the time duration of the thermal The discharge was performed immediately after finishing the charge for all cases considered. Furthermore, the behaviour of the temperature distribution inside the storage medium and the formation of two melting/solidification fronts were analysed. The evolution of a second front during the discharging process starting from an initial condition in which a certain amount of solid PCM has already formed inside the TES was evaluated.

2 Materials and methodology

2.1 Materials

In the present study, d-mannitol was selected as the PCM because of its suitability for medium temperature applications [20,21]. d-Mannitol is a sugar alcohol that is generally used in the food and pharmaceutical industries, but lately, it has been widely studied in LHTES applications due to its favourable thermal properties [22–24]. In the LHTES unit adopted in this work, a total mass of 0.83 kg of d-mannitol was used, whereas its main thermophysical properties are reported in Table 1.

The silicon fluid Syltherm 800 [25] was selected as a HTF considering a constant flow rate of 0.03 m^3/h for both the charge and discharge. The HTF temperature at the inlet of the storage device was chosen equal to 180 and 100 °C for charge and discharge, respectively, with a flow direction from top to bottom during both processes. This temperature values represent the initial condition at the HTF tube inlet. This value was considered constant for the entire duration of the test (without any deviations) because of the lack of experimental data. This consideration is valid for the boundary, while in the subsequent cells of the mesh, the temperature was calculated considering HTF dynamics and heat transfer between the HTF, tube wall and PCM.

Table 1. Properties of d-mannitol used in the numerical simulation [24].

	Solid	***Liquid***
Density (kg/m^3)	1400	1390
Specific heat (kJ/kg·K)	1.62	2.85
Thermal conductivity (W/m·K)	0.5	0.42
Kinematic viscosity (m^2/s)	-	2.84×10^{-5}
Phase change temperature (°C)	167[a]	
Phase change temperature range[*]	3	
Latent heat (kJ/kg)[*]	234	
Coefficient of thermal expansion [1/K]	6.11×10^{-4}	

[a]Mehling H. and Cabeza L. F. [26].
[*]Values obtained as the average of the experimental results found in the literature [1,15,21,22,24,27].

2.2 System geometry

A lab-scale storage system configured as a concentric tube heat exchanger is selected as a case study, in which the annulus space is filled with PCM and the heat transfer fluid flows from top to bottom in the inner tube during both charging and discharging process. This system has the same geometric characteristics as a real prototype used in previous experimental studies [19].

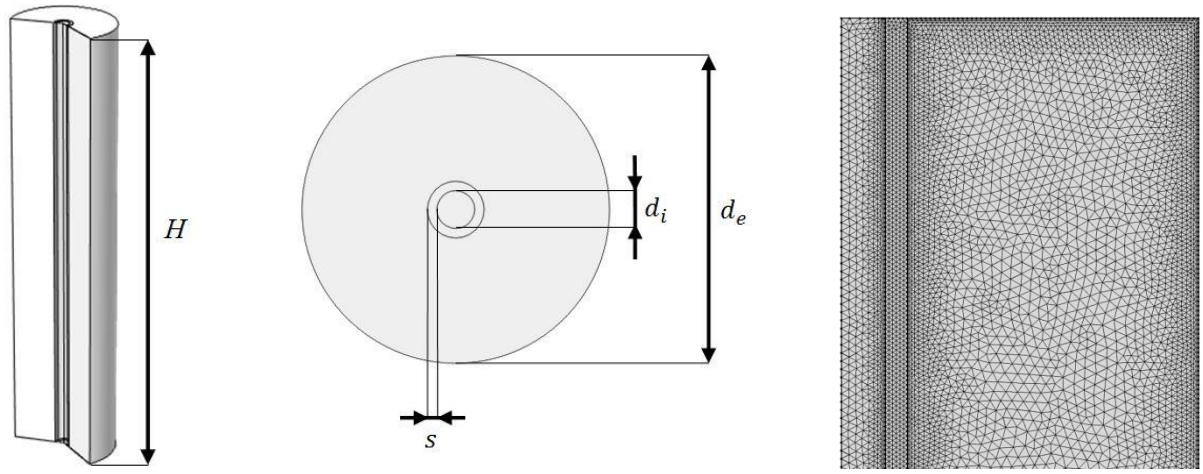

(a) (b) **(c)**

Fig. 1. TES system geometry configuration: (a) axial cross section; (b) top view; (c) adopted unstructured mesh at the top-height cross section of the model.

Therefore, the opportunity to use the same test case to experimentally validate the numerical results obtained in this study influenced the choice of this particular geometry. Of course, storage systems adopted in real applications are based on more complex geometries, but in this study, a model previously validated was selected to investigate the concept of partial load despite knowing that in the current form it might be not extrapolable to real cases applications. Moreover, the double-pipe configuration is considered as the elementary unit of a modular systems such as the shell-and-tube heat exchanger which, to date, is one of the most commonly used. Lastly, the laboratory scale TES unit adopted will allow for further experimental tests to be carried out using different configurations, different PCMs and different operating conditions. Figure 1 presents a schematic representation of the TES system, while its geometrical characteristics are reported in Table 2.

Table 2. Geometrical characteristics of the TES system.

Description	***Symbol***	***Units***	***Value***
Heat transfer surface	A_{surf}	m^2	$1.131 \cdot 10^{-4}$
Internal diameter HTF tube	d_i	Mm	8
External diameter tube PCM	d_e	Mm	65
Height	H	Mm	260
Tube thickness	s	Mm	2

2.3 Methodology

The present study investigates the effect of the partial load operating conditions on the performance of a LHTES system. This issue was developed focusing the analysis on two essential parameters, the duration of the TES cycle and the energy stored and released by the PCM considering the charging and discharging processes first separately and subsequently considering the overall outcome of the two processes.
Hence, four different charging and discharging processes were simulated, which only differ on the percentage of charge at which the process is stopped: 100% (Case 1: baseline), 95% (Case 2), 90% (Case 3) and 75% (Case 4). This percentage of charge coincide with the melting fraction inside the TES system, thus Case 1 is characterized by a complete melting of the PCM that correspond to a MF=1, while Case 2, Case 3 and Case 4 are characterized by partial charging process which correspond to a MF=0.95, MF=0.9 and MF=0.75 respectively. Despite knowing that partially charging the LHTES system is translated to a lower energy stored since the melting enthalpy won't be completely exploited, the reduction in process periods might be interesting when these systems are used. Thus, the melting fraction values close to the melting of the whole PCM inside the TES (full charging, MF=1) are selected as they represent the most interesting operating condition for real applications. These different states are selected as the initial conditions for the following discharging processes, which are set to start directly after the end of the charge and they are stopped at 1200 min imposed for the entire charging/discharging process of all cases analysed. This limit corresponds to the condition in which the heat transfer between the HTF and PCM is negligible. To characterise the four study cases, the values of percentage of charge were identified by their corresponding melting fraction during the charge, which is defined as the ratio between the PCM volume in the liquid phase in front of the total PCM volume. This parameter varies from 0, when the whole PCM is in the solid phase, to 1, when the whole PCM is in the liquid phase. Therefore, the condition in which the charge is stopped is established here by the melting fraction (MF).

The charging process starts from a homogeneous initial state of the TES system in order to achieve uniform HTF, tube wall and PCM domains at an initial set temperature of 100 °C. Then, at the beginning of the charging process, the HTF enters in the TES with an inlet temperature of 180 °C. The duration of the charge depends on the final melting fraction considered, while the discharge starts immediately at the end of the charge. Thus, at the beginning of the discharge, the HTF enters in the TES system with an inlet temperature of 100 °C. The HTF volumetric flow rate is 0.03 m^3/h and enters in the TES from the top during both charge and discharge and for all adopted cases.

3 Numerical model

A two-dimensional axisymmetric numerical model was developed with the COMSOL Multiphysics 5.0 platform to simulate the entire LHTES system behaviour during the phase transition processes, based on the

work carried out by Groulx et al. [28–31]. As mentioned, the mathematical model was validated in previous works [20,21] using the same geometrical configuration, with a good agreement between numerical and experimental results. In particular, temperature deviations of the same order of magnitude of the measurement uncertainty were evidenced considering natural convection in the PCM domain.

3.1 Governing equations

Three different domains were defined to develop the model: the HTF, wall tube and PCM [32,33]. To simulate the dynamic behaviour of the HTF flowing inside the inner tube, the continuity equation (1) and the momentum equation (2) were used.

$$\frac{\partial \rho}{\partial t} + \nabla \cdot (\rho \boldsymbol{u}) = 0 \tag{1}$$

$$\frac{\partial \rho \boldsymbol{u}}{\partial t} + \rho(\boldsymbol{u} \cdot \nabla)\boldsymbol{u} - \nabla \cdot \left[\mu\left(\nabla \mathbf{u} + (\nabla \mathbf{u})^{\mathrm{T}}\right)\right] + \nabla P = \boldsymbol{F} \tag{2}$$

In Equations (1) and (2), ρ and μ are the density and the dynamic viscosity of the HTF, respectively, $\mathbf{u}$ is the velocity vector, P is the pressure, T is the absolute temperature and t is time. The flow is considered laminar and incompressible and the effect of gravity is negligible ($F = 0$). Heat transfer from the HTF to the wall of the steel tube takes place by convection. The energy equation (3) was solved using the velocities found from the solution of Equations (1) and (2). In Equation (3), C_p and k are the specific heat and thermal conductivity of the material, respectively.

$$\rho C_p \frac{\partial T}{\partial t} + \rho C_p \boldsymbol{u} \cdot \nabla T = \nabla \cdot (k \nabla T) \tag{3}$$

Heat transfer from the wall of the steel tube to the PCM takes place by conduction, thus, Equation (3) was used neglecting the convective term. Finally, Equations (1), (2) and (3) were used to model the transient behaviour of the PCM during the entire charging and discharging processes by accounting for both conduction heat transfer in the solid PCM and conduction/natural convection heat transfer mechanisms in the liquid PCM, as better explained in section 3.4.

3.2 Boundary conditions

The numerical model is developed using the geometry presented in Figures 1(a) and (b), while the following initial and boundary conditions are considered:

- The outer wall of the TES system is assumed adiabatic.
- Initial temperature of the entire system (HTF, tube and PCM) is 100 °C.
- No-slip conditions on the tube surfaces.
- Laminar flow.
- Empirical functions describe viscous losses.
- Uniform inlet temperature of the HTF at the beginning of both charging and discharging process.

3.3 Model mesh

The adopted mesh is an unstructured grid and consists of 52828 triangular elements and 4236 quadrilateral elements, as reported in Figure 1c, with an average element quality of 0.9018 in order to achieve a mesh-independent result.

3.4 Numerical resolution

The phase change process was modelled using the energy equation (3) in accordance with the apparent heat capacity formulation (4). In this formulation, the latent heat L_f is introduced as an additional term in Equation (4) and it is assumed that the phase transition occurs in a temperature range between (T_m −

$\Delta T_m/2)$ and $(T_m + \Delta T_m/2)$. In this range, the material phase is modelled by a smoothed function θ, representing the fraction of phase before transition. The value of this function is equal to 0 for temperatures lower than $(T_m - \Delta T_m/2)$ and to 1 for temperatures higher than $(T_m + \Delta T_m/2)$. Figure 2 shows the evolution of modified $C_p(T)$ during the phase change process. The values of $C_p(T)$ related to solid and liquid phases of the PCM as well as the range of phase transition temperature, which was established assuming $\Delta T_m = 3\ °C$, are reported in Table 1.

$$C_p = \frac{1}{\rho}\left[(1-\theta)\rho_{phase1}C_{p,phase1} + \theta\rho_{phase2}C_{p,phase2}\right] + L_f\frac{\partial\alpha}{\partial T} \tag{4}$$

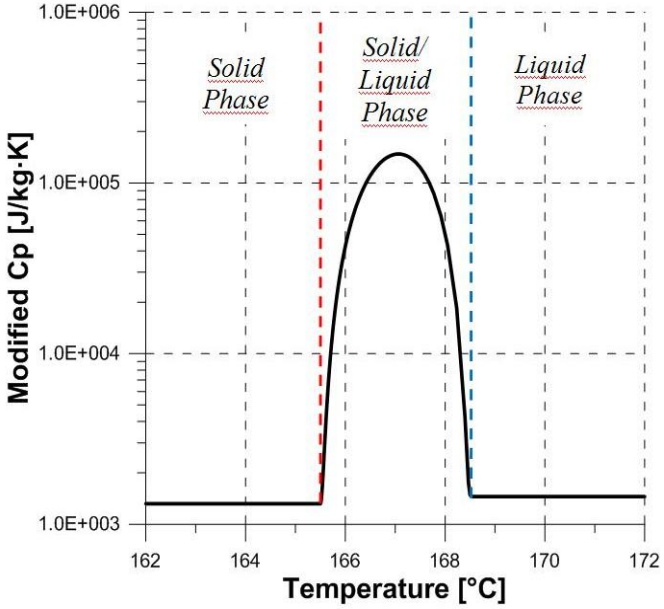

Fig. 2 - Modified $C_p(T)$ used in the model obtained by Equation (4)

The equivalent thermal conductivity and density of the PCM were obtained by Equations (5) and (6):

$$k = (1-\theta)k_{phase1} + \theta k_{phase2} \tag{5}$$

$$\rho = (1-\theta)\rho_{phase1} + \theta\rho_{phase2} \tag{6}$$

where α is the PCM mass fraction and is defined as [34]:

$$\alpha = \begin{cases} -1/2 & T < T_m - \Delta T_m/2 \\ \frac{1}{2}\dfrac{\theta\rho_{phase2} - (1-\theta)\rho_{phase1}}{\rho} & T_m - \Delta T_m/2 < T < T_m + \Delta T_m/2 \\ 1/2 & T > T_m + \Delta T_m/2 \end{cases} \tag{7}$$

The continuity (1) and momentum equations (2) were used to predict the behaviour of the PCM in the liquid phase. Two different volume forces were added to the momentum equation. The first was introduced to consider the buoyancy force giving rise to natural convection (Boussinesq approximation) according to Equation (8). In this equation, β, $\boldsymbol{g}$ and T_m are, respectively, the thermal expansion coefficient of the liquid PCM, the gravitational constant and the melting temperature, while ρ_l is the density of the PCM in the liquid state.

$$\boldsymbol{F_b} = \boldsymbol{g}\rho_l\beta(T - T_m) \tag{8}$$

In this method, the entire PCM was treated as a liquid, even when its temperature was lower than the melting one. This approach forces the Navier-Stokes equation to calculate the velocity everywhere, even when the PCM is in the solid phase. Thus, a second volume force F_v (9) was introduced in the momentum equation using the Carman-Kozeny equation (10):

$$\boldsymbol{F_v} = -A(T) \cdot \mathbf{u} \tag{9}$$

$$A(T) = A_{mush}\frac{(1-\theta)^2}{(\theta^3+\epsilon)} \tag{10}$$

where the constants A_{mush} and ϵ have values of 10^5 and 10^{-3}, respectively, according to Groulx et al. [30,31]. The parameter ϵ is used to avoid a division by zero when θ = 0 in the solid region.
The function $A(T)$ in Equation (10) assumes very large values when the melt fraction approaches 0, i.e., when the PCM is in the solid state, while it decreases towards zero when the melt fraction approaches 1, i.e., when the PCM is in the liquid state. The basic principle of F_v relates to a gradual increase in velocity from zero in the solid PCM to a finite value, which is calculated by Equation (2), in the liquid PCM. Furthermore, a modified viscosity was used to force the PCM in liquid state to behave as a solid when its temperature is lower than $(T_m - \Delta T_m/2)$ [30]. This parameter is obtained using Equation (11):

$$\mu(T) = \mu_l\big(1 + A(T)\big) \tag{11}$$

Thus, Equation (11) has a value equal to the viscosity of the liquid PCM when $T > (T_m + \Delta T_m/2)$ and an extremely large value when $T < (T_m - \Delta T_m/2)$. To study the effect of the partial load operating conditions on LHTES systems, important parameters, such as the melting fraction and energy stored and released during charging and discharging processes, were analysed. As discussed, the melting fraction is defined as the volume of PCM in the liquid phase divided by the total volume occupied by the PCM. Thus, its value is equal to 0 when the PCM is fully solidified and 1 when the PCM is fully melted. Although experimentally this parameter is difficult to evaluate, it is used in numerical analysis to easily obtain the percentage of charge or discharge for the whole duration of the process. With the purpose of analysing the complete storage cycle, the charging and discharging process were first evaluated separately and then combined while, to a better understanding, different definitions related to the rate of energy stored and released by the PCM during charge and discharge, respectively, were provided.
The numerical model reported above allows for the evaluation of the heat transfer within the three domains considered (HTF, tube and PCM) during the entire charging and discharging processes. In the overall assessment of the energy exchanged between HTF and PCM, the energy stored within the inner tube wall was considered negligible because of its small thickness. Thus, the energy released by the HTF corresponds to the energy absorbed by the PCM during charging, while the energy stored by the PCM corresponds to the energy absorbed by the HTF during discharge.
In general, the energy E released or absorbed by the HTF per unit of time during the charge and the discharge, respectively, is defined by Equation (12):

$$E = \int_{A_{in}} \rho \bar{u}_n C_p T dA - \int_{A_{out}} \rho \bar{u}_n C_p T dA \tag{12}$$

where, according to the assumption previously reported, E represents the energy stored and released by the PCM during the melting and solidification process, respectively. ρ, C_p and T are density, specific heat and temperature of the HTF, respectively, $\bar{u}_n$ is the velocity component normal to the cross-section, A is the tube cross-section area and the subscripts in and out refer to inlet and outlet tube cross-sections, respectively. Equation (12) was applied considering a fully developed laminar flow.

In order to better clarify and illustrate the results presented below, the following definitions are illustrated:

- E_{ch} is the energy stored by the PCM during the charge.
- E_{disc} is the energy released by the PCM to the HTF during the discharge.

- $E_{disc,res}$ is the residual stored energy, which indicates the rate of energy that can be still supplied by the PCM during the discharge when this process is stopped at a certain melting fraction value. Once the initial condition has been defined for each case considered, the *MF* identifies only one system energy state, thus, it is possible to establish a close correlation between the residual stored energy during the discharge and the *MF*.
- $E_{ch,un}$ is the amount of energy that the PCM would additionally store if instead stopping the charge at a certain value of *MF*, it is stopped at a $MF = 1$. In this work, the wording "unused stored capacity" is adopted.
- ROE_{disc} is the Ratio of Energy during discharge and it is defined as the ratio between the energy released during the discharge (E_{disc}) at the evaluated study case and the energy stored by the PCM at the end of the charge ($E_{ch,tot}$) for the baseline case.

$$ROE_{disc} = \frac{E_{disc}}{E_{ch,(MF=1)}} = \frac{E_{ch,tot} - E_{disc,res}}{E_{ch,tot}} \tag{13}$$

4 Results and discussion

Figures 3a and 3b show the correlation between the stored/released energy, the melting fraction and the duration of the complete thermal energy storage process. The knowledge of these properties' profiles at each instant allows for better management of the TES system, defining its wide potentialities.

Figure 3a reports the evolution of the *MF* during both charging and discharging processes. The upper curve (red) relates to the charge, while the labelled curves (blue) relate to discharge of the four study cases analysed. The figure also shows a map composed of dash-dotted curves, which refers to the percentage value of the ratio of energy during the discharge (ROE_{disc}). Thus, this map allows for evaluation of the state-of-the-charge, in terms of *MF*, of the TES system during the discharging process and consequently the duration of the discharge (or of the complete storage cycle including the charge), according to the amount of energy provided by the TES system to the user.

ROE_{disc} does not reach 100% (Figure 3a) because the end of the discharge occurs when a residual (albeit small) temperature difference between the PCM and the HTF still exists, rather than after the complete solidification of the PCM ($MF = 0$). Indeed, when this condition is reached, the energy released by the PCM is only in the form of sensible heat and its rate is indicated by the filled area of Figure 3b for the four cases considered.

In Figure 3a, it can be observed that the melting process takes longer than the solidification due to the lower temperature difference between the HTF temperature (180 °C at the entrance) and the phase change temperature of the PCM (167±1.5 °C), which causes the heat transfer rate to be lower than in the discharging process (HTF inlet temperature of 100 ºC). Notice that Case 1, which is the baseline case in which the $MF = 1$ was achieved, finishes after ~708 min. The *MF* values of 0.6 and 0.9 were reached in ~247 and 500 min, respectively, that is the 34.9% and the 70.6% of the time required for the complete melting. Moreover, in half of the time required to end the charge the melting fraction reaches a value higher than 0.75. It means that, in practice, it is convenient to stop the charging process before reaching the complete PCM melting ($MF = 1$). To prove and better define this statement, the amount of time saving, achieved under partial load operating condition, despite a certain reduction in the energy stored by the PCM during the charge (unused stored capacity) is evaluated below.

Figure 3b shows the evolution of the energy exchanged between the HTF and PCM during the whole process. In particular, the upper red curve represents the energy stored by the PCM during the charging process, while the labelled blue curves represent the energy released by the PCM during the discharge, and directly provide the value of the residual stored energy $E_{disc,res}$ given by Equation (13). This figure also shows a map composed of dash-dotted curves referred to constant values of melting fraction during the discharging process. Finally, as discussed, the filled part represents the rate of energy released by the PCM in the form of sensible heat after the complete solidification of the PCM. An energy amount of ~0.135 kWh is stored into the TES system when the complete PCM melting is reached, i.e., at the end of the charging process of Case 1. Obviously, partial load working conditions affect not only the duration of the process but also the energy stored/released by the TES system.

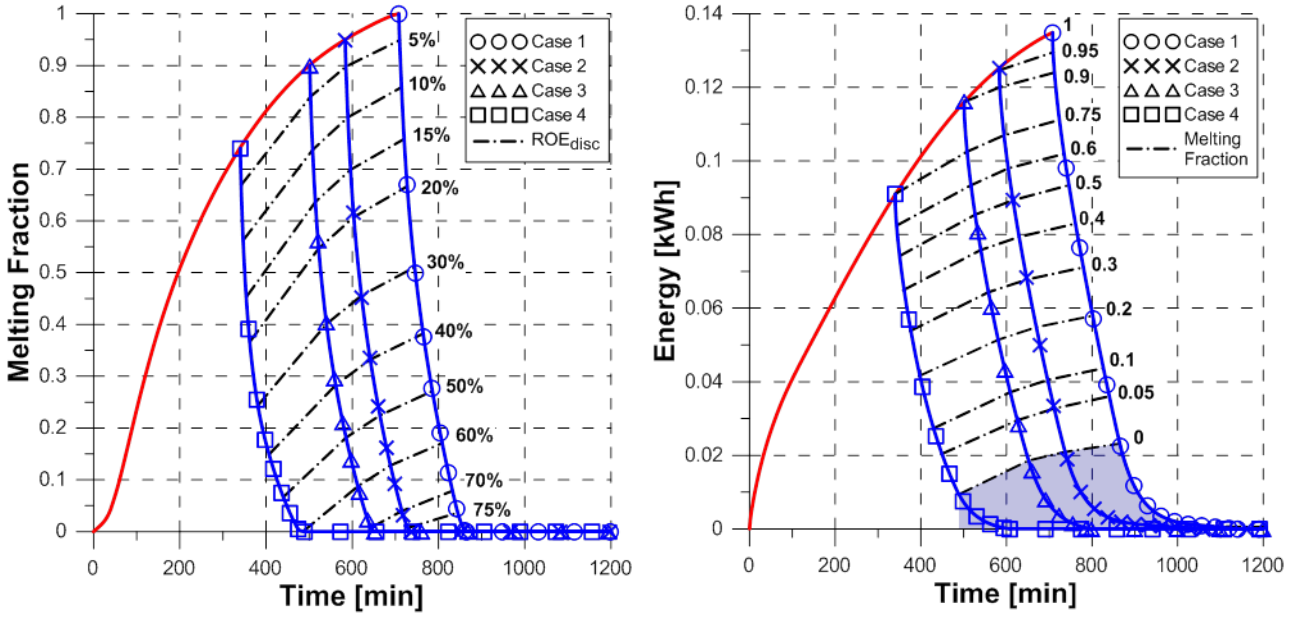

(a) **(b)**

Fig. 3. (a) PCM melting fraction evolution during the charge (red curves) and the discharge (blue curves) for the four case studies (labelled blue curves). The dash-dotted curves refer to the percentage value of the ratio of energy during the discharge (ROE_{disc}). (b) Evolution of the energy stored/released by the PCM during charge and discharge. The filled area represents the rate of energy released by the PCM in the form of sensible heat during the discharge and the dash-dotted curves refer to constant values of the melting fraction during the discharge.

In the following sections, using the information reported in Figures 3a and 3b, the charging and discharging processes were first analysed separately and subsequently considering the overall outcome of the two processes. Therefore, it is possible to evaluate the convenience of working in partial load operating conditions, by taking into account the TES process in its distinct phases or in its entirety. To carry out this investigation, fundamental parameters, such as stored/released energy and the duration of the processes, were considered.

Finally, the evaluation of temperature distribution and heat transfer rate released by PCM, as well as the evolution of the solidification front, were analysed during the discharge in order to evaluate the influence of partial load operating conditions on the solidification process.

4.1 Charging process

Figure 4 presents the percentage saved charge time and the unused energy in comparison to the baseline case as a function of the melting fraction. Stopping the charging process at melting fraction between 0.75 and 0.90 can save up to 30–50% of the charge time, with a consequent reduction in the unused storage capacity of ~15–30%. This result is very significant, since it allows for an optimum improvement in the management of LHTES systems with proper and suitable processing of the different phases of the thermal energy storage process.

Furthermore, it can be also noticed that the curves of both Figures 3a and 4 present a smooth slope trend for melting fraction values higher than 0.1. For these values, the HTF tube is completely surrounded by a layer of liquid PCM along its entire length. In fact, at the beginning of the charging process, the heat transfer is dominated by the high temperature difference between the hot HTF that enters the TES system and the cold PCM in the solid state.

Thereafter, when the PCM undergoes the phase transition along the entire wall of the inner tube, the heat transfer is affected by the presence of convective motions in liquid PCM and by a reduced temperature difference between PCM and HTF.

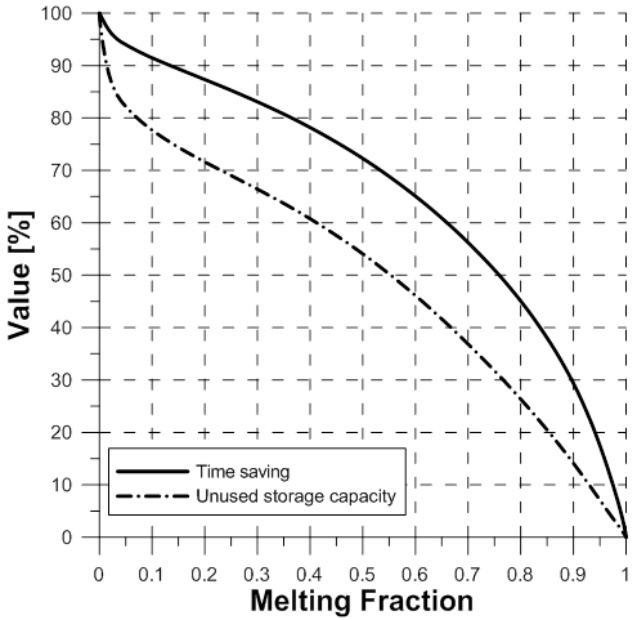

Fig. 4. Saved charge time and unused storage capacity as a function of the melting fraction during the charging process.

4.2 Discharging process

The dash-dotted curves, which refer to constant percentage values of ROE_{disc}, in Figure 3a and to a constant melting fraction in Figure 3b allow us to define an "operating map", useful for improving and optimising the TES processes. Indeed, during operation, it is not always necessary or possible to perform complete charging/discharging processes of the TES system due, for example, to unexpected peak loads, failures or random energy demands, or it simply not being favourable. Therefore, this map allows for the determination of the charge/discharge load conditions over time, which improves the management of the entire energy storage process. In other words, these maps allow us to evaluate the convenience of working under partial loads in order to determine the most suitable operating condition in terms of time duration of a complete cycle, when the maximum storage capacity of the TES device and the user energy requirement are defined. Figure 5a shows the ROE_{disc} only considering the duration of the discharge. The four cases present the same behaviour up to a percentage value of ROE_{disc} of 25% (after about the first 30 min of discharge time). Indeed, at the beginning of the discharge, the solidification front and, in general, the thermal storage process develops in the same way for all considered cases (the PCM solidifies around the inner tube). After this threshold, the final condition of the charge, which depends on the chosen charge percentage value, influences the process by producing the differences for a given discharge time, as shown in Figure 5a.

Finally, as stated previously, the value of ROE_{disc} does not reach 100% because after the end of the solidification process, the heat transfer mechanisms are only by sensible heat. As an example, at the end of the solidification (thus, only latent heat is accounted for) of Case 4, the ROE_{disc} is ~60% (see also Figure 3a), while a discharge time difference of ~48 min exists between Cases 1 and 4, considering the same ROE_{disc} value.

In Figure 5b, the heat transfer rate released by the PCM during the discharging process was analysed for a better comprehension of the TES system behaviour under partial load operating conditions. In fact, the four cases analysed were characterised by different temperature distributions (Figure 6) and, consequently, by different melting fractions due to their different initial conditions at the beginning of the discharge. For a clearer representation, only the first 240 min were reported, since after this time, the heat transfer rates show negligible differences, tending to zero at the end of the discharge. At the beginning, the heat transfer process involves mainly the sensible heat of the liquid phase, similar for all four cases. Conversely, the partial load condition strongly affects the heat transfer rate after ~30–40 minutes, when the phase transition occurs, due to the different temperature distributions at the end of the charge, as reported in Figure 6. At this stage, the process involves mainly the residual latent heat up to the complete PCM solidification. Finally, the heat transfer rate depends only on the sensible heat of the PCM in the solid phase after ~140–150 min.

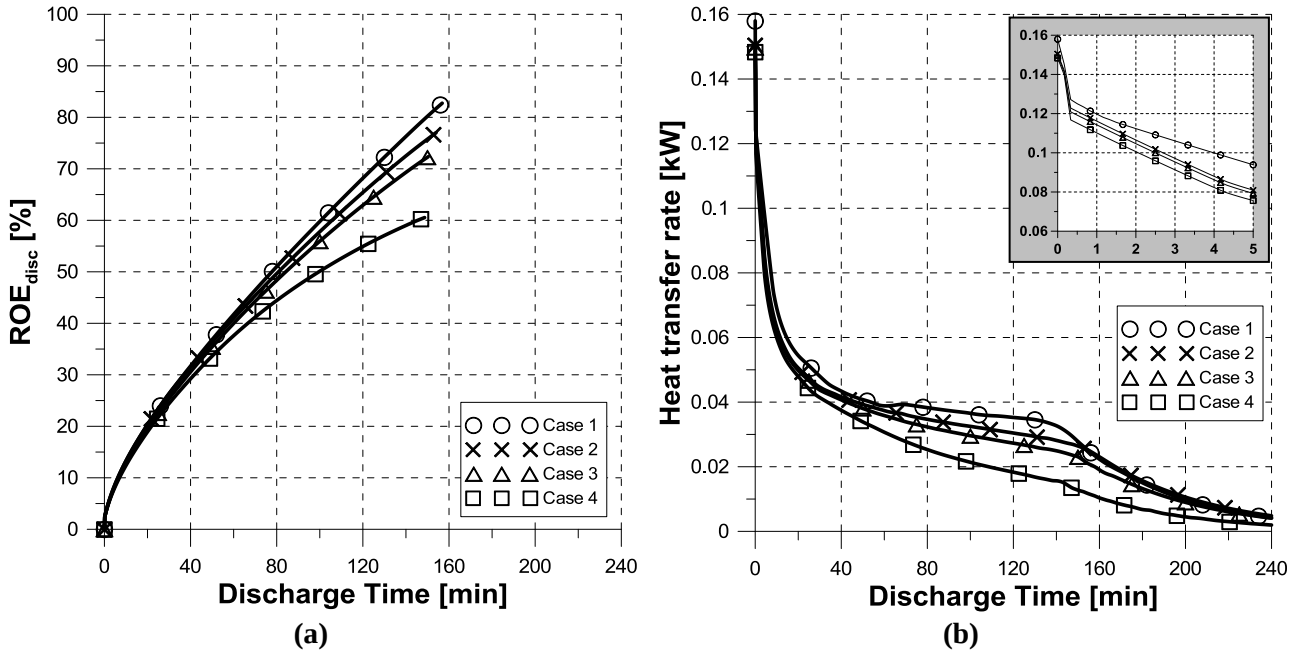

Fig. 5. (a) ROE_{disc} as a function of the discharge time (only latent heat is accounted for). (b) Evolution of the heat transfer rate released by PCM during the discharging process.

The results show that Case 1, exploiting the higher amount of melted PCM generated during the charge phase, provides a higher thermal power to the HTF during the discharge with respect to the others cases, almost double with respect to Case 4. Thus, working under total load operating conditions (Case 1) is the most suitable solution when more thermal power is required by the user.
Alternatively, working under partial load conditions provides the same value of ROE_{disc} with considerable time saving in continuous operation, in which both charge and discharge are cyclically performed, as shown in Figure 3a. The analysis of the correlation between time saving and the ROE_{disc} during the complete storage cycle was conducted more in detail in section 4.3.Concerning the temperature distribution inside the TES system, Figure 6 shows the situation at the end of charge that is at the beginning of discharge.

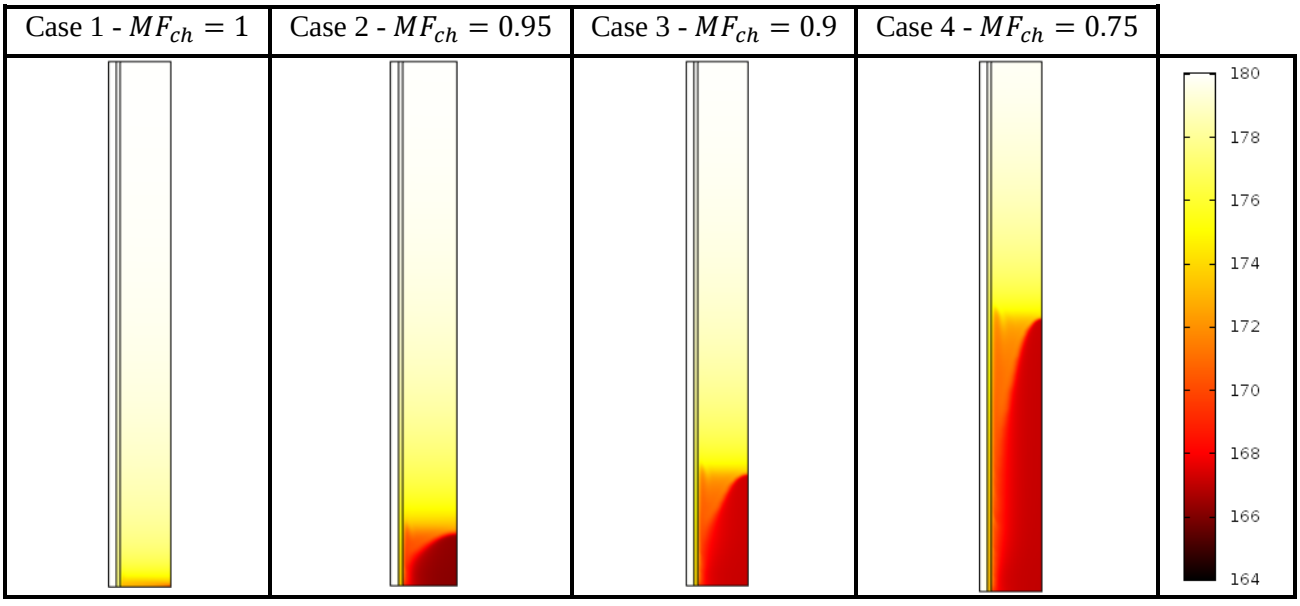

Fig. 6. Temperature distribution within the TES system at the beginning of the discharging process.

The PCM placed in the upper part of the TES is in the liquid state in all cases and it is characterised by a temperature much higher than the phase transition temperature, as it is closer to the HTF inlet.

Conversely, considerable temperature differences were detected in the lower part of the TES system, depending on the partial load operating condition. in Case 1, the PCM is completely in the liquid phase, while the lower the values of the melting fraction at the end of the charge, the higher the area affected by temperatures below the range of the phase transition, involving almost half the height of the TES system in Case 4.

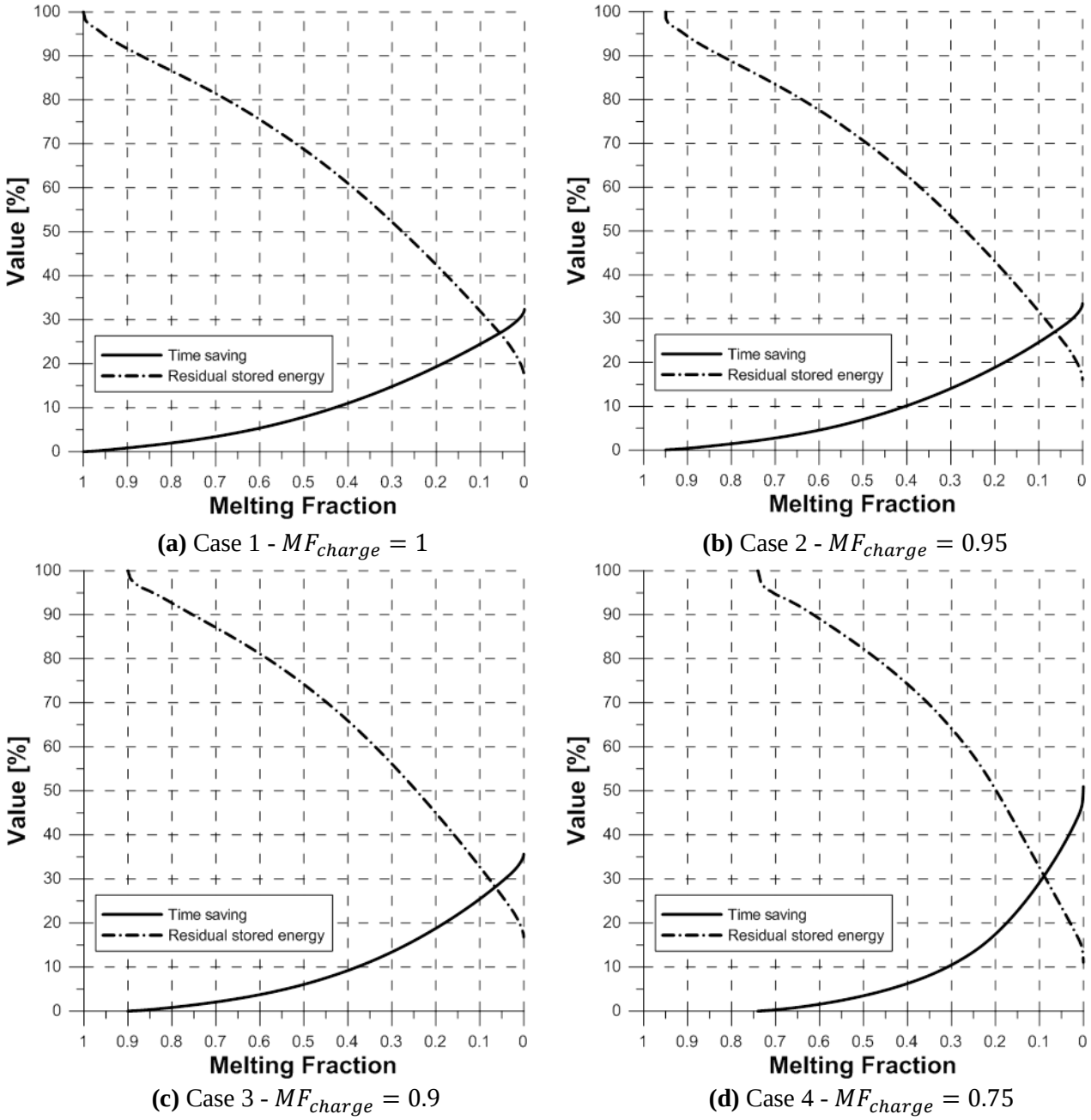

(a) Case 1 - $MF_{charge} = 1$ **(b)** Case 2 - $MF_{charge} = 0.95$

(c) Case 3 - $MF_{charge} = 0.9$ **(d)** Case 4 - $MF_{charge} = 0.75$

Fig. 7. Saved discharge time and residual stored energy as a function of the melting fraction during the discharging process.

By analysing separately the four cases considered, the percentage values of the saved discharge time (the charge time is not accounted for) and the percentage values of the corresponding residual stored energy $E_{disc,res}$ as a function of the melting fraction are reported in Figure 7. Notice that the melting fraction varies from the actual value at the end of the charging process (that is at the beginning of the discharge), to zero, which corresponds to the complete PCM solidification. It is important to highlight that, for $MF = 0$, the discharging process is not complete and a residual stored energy is still present, only consisting of sensible heat, in the order of ~16–17% for Cases 1, 2 and 3 (Figures 7a–c) and of ~11% for Case 4 (Figure 7d).

Consequently, the time saving gained by waiving to recover this small share of sensible heat is between 32–35% for Cases 1, 2 and 3 and ~49% for Case 4.

4.3 Complete storage cycle (charge and discharge)

In the previous two sections, the charging and discharging processes were discussed separately. However, by analysing the discharge in Figures 3a and 3b, considerable time differences, in terms of overall charge/discharge duration, exist between Case 1 (baseline case) and the others to attain the same energy released by the PCM. Therefore, a more effective management, in terms of time duration, could be pursued by operating under partial load conditions, taking into account the complete thermal storage cycle, which means performing the charge until the complete melting of PCM ($MF = 1$) and successively the discharge. Thus, partial load operating conditions could be a fundamentally key in the continuous and cyclical working operation of the LHTES system. This aspect can be better assessed by analysing Figure 8, which reports the percentage values of the total time saved (taking into account overall charge/discharge duration) as a function of ROE_{disc} for Cases 2, 3 and 4 compared to Case 1. In this baseline case, the maximum energy stored during the charge, which is equal to that released by the PCM during the discharge, is 0.135 kWh, while the time required to achieve a complete melting of the PCM is equal to 708 min. Thus, considering a requirement equal to 50% of the maximum energy potentially releasable by the PCM during the discharge, a time saving of ~44% for Case 2, 25% for Case 3 and 15% for Case 4 is obtained by working in partial load conditions with respect to total load conditions (Case 1).

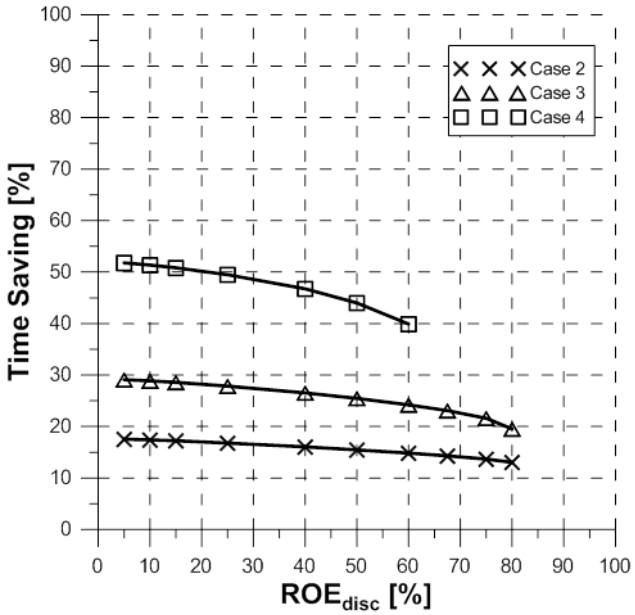

Fig. 8. Total saved time (considering the overall charge/discharge duration) as a function of ROE_{disc} compared to Case 1.

4.4 Residual energy and time saving

The charging and discharging processes present different durations due to the temperature difference between the HTF inlet temperature at the beginning of the charge (180 °C) and discharge (100 °C), and the PCM phase transition temperature (167±1.5 °C). By analysing only the discharge (see also Figure 3a), the complete solidification, with an HTF inlet temperature of 100 °C, takes ~157 min for Case 1 and ~149 min for Case 4. Thus, the discharging process duration takes only ~5.2% less time when starting from a melting fraction of 0.75 with respect to 1. However, the dash-dotted curves reported in Figure 3b show that an important share of the discharge time is required to solidify the last 0.1 of the liquid PCM, although a noticeable slope variation of the discharge curves can be already observed when the melting fraction approaches 0.3. Table 3 reports the percentage values of the saved discharge time with respect to the overall discharge time (the charge time is not accounted for) and of the residual stored energy $E_{disc,res}$ when the discharge is stopped for a melting fraction equal to 0.1. Table 3 also reports the percentage share of sensible heat in the residual stored energy $E_{disc,res}$. This means that, for example, in Case 1, when $MF = 0.1$ was

reached during discharge, the 51.8% of the residual store energy (i.e., 32.4% of the maximum stored energy in the TES system) is sensible heat. Thus, the incidence of sensible heat in the amount of residual energy $E_{disc,res}$ can be assessed when $MF = 0.1$ was reached during the discharge.

The results from Table 3 show that saved time increases from ~24.5% in Case 1 to ~27.9% in Case 4, while the residual stored energy $E_{disc,res}$ is of the order of 31–32% in all cases. Hence, although it may be convenient in terms of time saving, the fact of working in partial load conditions during the discharge and stopping it before complete solidification (when $MF = 0.1$ as a reference), the amount of the residual stored energy that could still be provided by the TES system is quite significant. Therefore, these considerations show how a proper evaluation of process parameters, such as time duration and energy exchanged, is important in order to identify optimal management criteria of the system. Moreover, it must be observed that this residual energy $E_{disc,res}$ also includes the rate of thermal energy stored in the form of sensible heat, evidenced by the filled area reported in Figure 3b.

Table 3. Saved discharge time, residual stored energy $\boldsymbol{E_{disc,res}}$ and the corresponding share of sensible heat when stopping the discharging process at $\boldsymbol{MF = 0.1}$.

	Saved time [%]	$\boldsymbol{E_{disc,res}}$ ***[%]***	***Share of sensible heat [%]***
Case 1	24.5	32.4	51.8
Case 2	24.6	32.1	50.2
Case 3	25.5	31.8	50.1
Case 4	27.9	31.2	34.1

4.5 Phase front evolution

Figure 9 shows the phase change evolution during the discharging process of the four cases considered for different values of the MF. The red area represents the solid PCM, while the blue area represents the liquid PCM. Thus, in these figures, the *MF* varies from the initial condition of the discharge (that corresponds to the end of the charge) represented by the first image, and decreases to values equals to 0.5, 0.25 and 0.1, represented by the others three images, respectively. It can be noticed that the solid fraction at the beginning of the discharge affects the shape of the solid-liquid front established inside the TES system. For a $MF_{disch} = 0.5$, a single solid-liquid interface is observed for Case 1, while two different solid-liquid fronts are present in the other three cases.

The first front, confined to the bottom of the peripheral wall, is due to the amount of solid PCM still existing at the end of charge, which slowly continued to the melt because of the higher PCM temperature of its surroundings. The second one develops growing around the inner tube when beginning the discharge. For $MF_{disch} = 0.25$, the two fronts are still clearly detectable for Case 4 and barely discernible in Case 3, while they are incorporated with each other in Case 2. Subsequently, for $MF_{disch} = 0.1$, the two fronts merge completely in all cases forming a single boundary, while a liquid PCM volume remains confined to the wall of the TES outer tube.

The shape of this volume affects the slope of the melting fraction curves (Figure 3a), of the energy released by the PCM during discharge (Figure 3b) and of the time saving curves (Figure 8). In fact, the liquid PCM covers the whole area along the entire length of the outer tube of the TES system for Case 1 (Figure 9a), while this area progressively decreases in the other cases (Figures 9b–d).

This occurrence obviously affects the heat transfer process required to complete the solidification of the same amount of liquid phase and, consequently, the TES system performance at partial load operating condition during discharge is sensibly affected by the initial state of the system at the beginning of this phase.

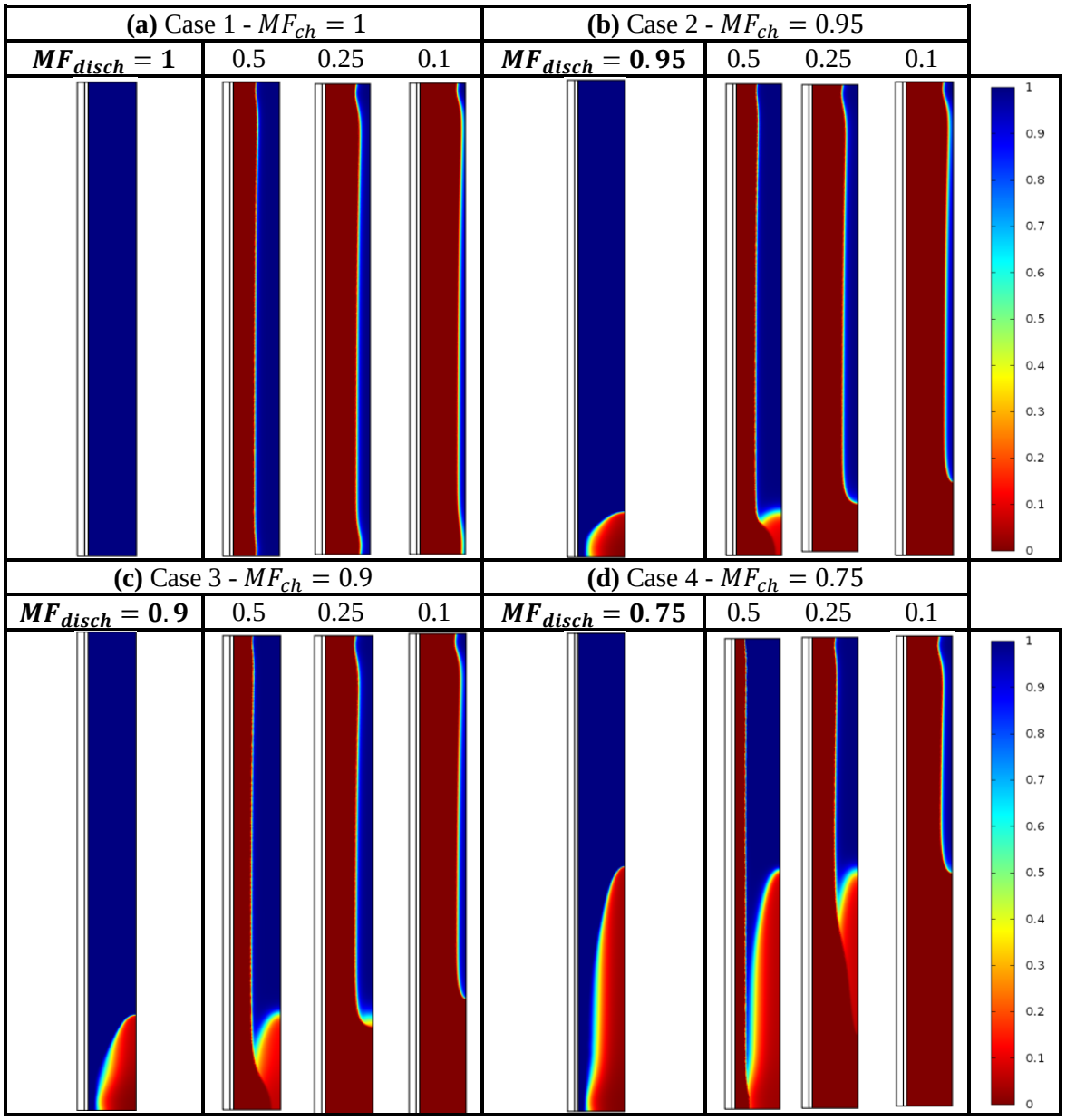

Fig. 9. Phase evolution at a certain melting fraction values for all cases considered.

5 Conclusions

Operation at partial load conditions is a fundamental aspect in industrial applications coupled to LHTES systems since it is not always favourable, necessary or possible to perform complete charge and discharge cycles. This issue is investigated in the present study for a simple LHTES system analysing two essential parameters, the duration of the TES cycle and the energy stored and released by the PCM during the charging and discharging processes. Four different cases, referred to different values of melting fraction during the charge, were selected as the initial condition of the discharge.

Characteristic curves of time saving and unused energy storage capacity during charge and residual stored energy during discharge as a function of melting fraction are obtained. Despite full load operation allows to obtain higher heat transfer rate during both charging and discharging processes, due to the different temperature distribution within the TES system, this study clearly evidences that partial load operating conditions allow a considerable reduction in the charging and discharging duration processes. It was found that stopping the charge to values of the melting fraction between 0.75 and 0.90 can result in great advantages in terms of time saving (up to 50%) with a limited amount of the unused storage capacity (up to 30%). On the contrary, if the discharge is stopped when it reaches a melting fraction of 0.1, the amount of residual stored energy is about the order of 30–32% in all cases and the consequent reduction in the discharge time varies between 24.5% and 27.9% for Case 4. In addition, residual stored energy between 11%

and 16% were achieved by stopping the discharge at the end of the solidification process (melting fraction equal to 0), with a consequent reduction in the discharge time between 32% and 49%.
Detailed maps consisting of characteristic curves related to constant values of melting fraction and ROE_{disc} are obtained. These maps allow evaluating the convenience of operating in partial loads operating conditions denoting the most efficient load condition (charge/discharge) to satisfy a specific energy demand. Moreover they provide an accurate decision-making strategy for LHTES systems when they are adopted in real applications. Furthermore, the PCM phase evolution inside the TES system is evaluated. Two different solid-liquid fronts exist within the storage device during discharge since the residual value of the melting fraction at the end of the charge influences the progress of these two fronts. An accurate analysis of this work leads to the assertion that the validity of the results obtained is closely related to the particular geometry of the TES system adopted and on the initial temperature of the HTF for charging and discharging processes, as well as on the properties of the PCM selected. The TES system adopted in this paper is based on a lab-scale device configuration which consists of a double-pipe heat exchanger even though full-scale solutions are usually based on more complex geometries. Therefore, it can be assumed that the results obtained have general validity in qualitative terms when considering different configurations of the storage system representing a consistent methodology for the study of partial loads operating condition in PCM-TES systems. In this sense, the use of a simple test case is framed as the first step to address the issues related to partial load working conditions and evaluate the impact of others important factors, such as temperature, TES size and shape and PCM material. In the methodology proposed in this paper, the melting fraction is the fundamental parameter used to define the state-of-charge of the system during the entire storage cycle. Although the evaluation of melting fraction is easily achievable in numerical simulation studies, it turns out to be rather complicated in experimental tests. In this context, the enthalpy variation could be used to identify the correct state-of-charge of the system during the charging and discharging processes to avoid the difficulty of the *MF* evaluation. Finally, it is important to highlight how these considerations allow to understand not only the complexity of LHTES systems but also all their potential when adopted in real applications. Indeed, the significant impact on the storage capacity that characterizes the different operating conditions during melting/solidification processes appears to be an important factor in the evaluation of the system design, operation and control.

Acknowledgements

Simone Arena and Efisio Casti would like to thank the Department of Mechanical, Chemical and Materials Engineering of the University of Cagliari for their founding research grants. The work was partially funded by the Spanish government (ENE2015-64117-C5-1-R (MINECO/FEDER)). The authors would like to thank the Catalan Government for the quality accreditation given to their research group (2014 SGR 123). GREA is certified agent TECNIO in the category of technology developers from the Government of Catalonia. Jaume Gasia would like to thank the Departament d'Universitats, Recerca i Societat de la Informació de la Generalitat de Catalunya for his research fellowship (2017 FI_B1 00092).

References

[1] A. Gil, M. Medrano, I. Martorell, A. Lázaro, P. Dolado, B. Zalba, L.F. Cabeza, State of the art on high temperature thermal energy storage for power generation. Part 1-Concepts, materials and modellization, Renew. Sustain. Energy Rev. 14 (2010) 31–55.
[2] S.M. Hasnain, S.H. Alawaji, M.S. Smiai, Prospects of cool thermal storage utilization in Saudi Arabia, Energy Convers. Manag. 41 (2000) 1829–1839.
[3] Al-qalamchi, A.W. Adnan, A. Ansam, Performance of ice storage system utilizing a combined partial and full storage strategy, Desalination. 209 (2007) 306–311.
[4] S. Sanaye, M. Hekmatian, Ice thermal energy storage (ITES) for air-conditioning application in full and partial load operating modes, Int. J. Refrig. 66 (2016) 181–197.
[5] J. Xu, R.Z. Wang, Y. Li, A review of available technologies for seasonal thermal energy storage, Sol. Energy. 103 (2014) 610–638.
[6] M.M. Rahman, M.G. Rasul, M.M.K. Khan, Feasibility of thermal energy storage systems in an institutional building in subtropical climates in Australia, Appl. Therm. Eng. 31 (2011) 2943–2950.
[7] K. Nithyanandam, R. Pitchumani, A. Mathur, Analysis of a latent thermocline storage system with encapsulated phase change materials for concentrating solar power, Appl. Energy. 113 (2014) 1446–1460.
[8] B. Zhao, M. Cheng, C. Liu, Z. Dai, Cyclic thermal characterization of a molten-salt packed-bed

thermal energy storage for concentrating solar power, Appl. Energy. 195 (2017) 761–773.
[9] D. Macphee, I. Dincer, Performance assessment of some ice TES systems, Int. J. Therm. Sci. 48 (2009) 2288–2299.
[10] B. Delcroix, M. Kummert, A. Daoud, Thermal behavior mapping of a phase change material between the heating and cooling enthalpy-temperature curves, Energy Procedia. 78 (2015) 225–230.
[11] F. Ferrara, A. Gimelli, A. Luongo, Small-scale concentrated solar power (CSP) plant: ORCs comparison for different organic fluids, Energy Procedia. 45 (2014) 217–226.
[12] E.G. Bennouna, A. Mimet, H. Frej, Thermal Storage System Development for a 1 MW CSP Pilot Plant Using an Organic Rankine Cycle, in: EuroSun 2014, ISES Conf. Proc., Aix-les-Bains (France), 2014.
[13] D. Krüger, A. Kenissi, S. Dieckmann, C. Bouden, A. Baba, A. Oliveira, J. Soares, Pre-design of a mini CSP plant, Energy Procedia. 69 (2015) 1613–1622.
[14] J. Gasia, L. Miró, L.F. Cabeza, Review on system and materials requirements for high temperature thermal energy storage. Part 1: General requirements, Renew. Sustain. Energy Rev. 75 (2017) 1320–1338.
[15] E. Oró, A. Gil, L. Miró, G. Peiró, S. Álvarez, L.F. Cabeza, Thermal energy storage implementation using phase change materials for solar cooling and refrigeration applications, Energy Procedia. 30 (2012) 947–956.
[16] B.P. Tripathi, V.K. Shahi, Progress in Polymer Science Organic-inorganic nanocomposite polymer electrolyte membranes for fuel cell applications, Prog. Polym. Sci. 36 (2011) 945–979.
[17] C. Park, K.J. Kim, J. Gottschlich, Q. Leland, High performance heat storage and dissipation technology, in: ASME Int. Mech. Eng. Congr. Expo., Orlando, Florida, USA, 2005.
[18] C. Vannoni, R. Battisti, S. Drigo, Potential for Solar Heat in Industrial Processes, in: IEA SHC Task 33, SolarPACES Task IV Sol. Heat Ind. Process., 2008.
[19] M. Medrano, M.O. Yilmaz, M. Nogués, I. Martorell, J. Roca, L.F. Cabeza, Experimental evaluation of commercial heat exchangers for use as PCM thermal storage systems, Appl. Energy. 86 (2009) 2047–2055.
[20] J. Pereira, P. Eames, Thermal energy storage for low and medium temperature applications using phase change materials – A review, Appl. Energy. 177 (2016) 227–238.
[21] A. Gil, E. Oró, G. Peiró, S. Álvarez, L.F. Cabeza, Material selection and testing for thermal energy storage in solar cooling, Renew. Energy. 57 (2013) 366–371.
[22] G. Kumaresan, R. Velraj, S. Iniyan, Thermal Analysis of D-mannitol for Use as Phase Change Material for Latent Heat Storage, J. Appl. Sci. 11 (2011) 3044–3048.
[23] A. Solé, H. Neumann, S. Niedermaier, I. Martorell, P. Schossig, L.F. Cabeza, Stability of sugar alcohols as PCM for thermal energy storage, Sol. Energy Mater. Sol. Cells. 126 (2014) 125–134.
[24] M. Shibahara, Q. Liu, K. Fukuda, Heat transfer characteristics of d-mannitol as a phase change material for a medium thermal energy system, Heat Mass Transf. 52 (2016) 1993–2004.
[25] Dow Company, Syltherm800 - product brochure, (n.d.) 1–28.
[26] H. Mehling, L.F. Cabeza, Heat and cold storage with PCM: an up to date introduction into basics and applications, 2008.
[27] A. Solé, H. Neumann, S. Niedermaier, I. Martorell, P. Schossig, L.F. Cabeza, Stability of sugar alcohols as PCM for thermal energy storage, Sol. Energy Mater. Sol. Cells. 126 (2014) 125–134.
[28] D. Groulx, R. Murray, Modeling Convection During Melting of a Phase Change Material, in: Proceeding COMSOL Conf., Boston, 2011.
[29] D. Groulx, W. Ogoh, Solid-Liquid Phase Change Simulation Applied to a Cylindrical Latent Heat Energy Storage System, in: Proceeding COMSOL Conf. Bost., 2009.
[30] D. Groulx, F. Samara, P.H. Biwole, Natural Convection Driven Melting of Phase Change Material: Comparison of Two Methods, in: COMSOL Conf., 2012: pp. 1–8.
[31] D. Groulx, A.C. Kheirabadi, The Effect of the Mushy-Zone Constant on Simulated Phase Change Heat Transfer, in: ICHMT Int. Symp. Adv. Comput. Heat Transf., Piscataway, USA, 2015.
[32] S. Arena, G. Cau, C. Palomba, CFD Simulation of Melting and Solidification of PCM in Thermal Energy Storage Systems of Different Geometry, J. Phys. Conf. Ser. 655 (2015).
[33] S. Arena, Modelling, design and analysis of innovative thermal energy storage systems using PCM for industrial processes, heat and power, PhD Thesis. (2015).
[34] Comsol, The Heat Transfer Module User's Guide, 2013.